



Article

Imidazo-Phenanthroline Ligands as a Convenient Modular Platform for the Preparation of Heteroleptic Cu(I) Photosensitizers

Marie-Ann Schmid ^{1,†}, Martin Rentschler ^{2,†}, Wolfgang Frey ², Stefanie Tschierlei ^{1,*}  and Michael Karnahl ^{2,*} 

¹ Institute of Inorganic Chemistry I, Ulm University, Albert-Einstein-Allee 11, 89081 Ulm, Germany; marie-ann.schmid@uni-ulm.de

² Institute of Organic Chemistry, University of Stuttgart, Pfaffenwaldring 55, 70569 Stuttgart, Germany; martin.rentschler@oc.uni-stuttgart.de (M.R.); wolfgang.frey@oc.uni-stuttgart.de (W.F.)

* Correspondence: stefanie.tschierlei@uni-ulm.de (S.T.); michael.karnahl@oc.uni-stuttgart.de (M.K.); Tel.: +49-731-50-22583 (S.T.); +49-711-685-64274 (M.K.)

† These authors contributed equally to this work.

Received: 20 November 2018; Accepted: 10 December 2018; Published: 12 December 2018



Abstract: The capture and storage of solar energy is a promising option to overcome current energy issues. To put such systems into practice, molecular photosensitizers should be based on abundant metals and possess a strong absorption capability for visible light. Therefore, a systematic series of four novel heteroleptic Cu(I) complexes of the type $[(P^*P)Cu(N^*N)]^+$ (with $P^*P = \text{xantphos}$ and $N^*N =$ different diimine ligands) has been prepared. As an essential feature, these copper photosensitizers contain an imidazole moiety at the backbone of the diimine ligand, which increases the aromatic π -system compared to phenanthroline type ligands. Moreover, 2-(4-bromophenyl)-1-phenyl-1*H*-imidazo-[4,5-*f*][1,10]phenanthroline was used as a starting point and modular platform for gradually extended diimine ligands. Suzuki cross-coupling was applied to introduce different kind of substituents in the back of this ligand. Afterwards, a combination of NMR spectroscopy, mass spectrometry, X-ray analysis, cyclic voltammetry, UV/vis and emission spectroscopy was used to investigate the structural, electrochemical and photophysical properties of these compounds. As a result, a reversible reduction, strongly increased extinction coefficients and significantly redshifted absorption maxima (>20 nm) were found compared to traditional Cu(I) photosensitizers without an imidazo moiety. Moreover, these compounds show a bright emission in the solid state.

Keywords: copper photosensitizers; imidazo-phenanthroline ligands; Suzuki coupling; X-ray analysis; photophysics; structure-property relationships

1. Introduction

The increased use of solar energy represents a promising option that might contribute to solving current energy challenges [1–6]. At present about 85% of global energy currently originates from fossil fuels, such as oil, gas and coal or nuclear power [2,4,5]. Beside their limitations, the burning of carbon-based fuels releases large amounts of carbon dioxide, which is a major reason for global warming. In contrast, the sun provides almost unlimited energy (approx. 3×10^{24} J per year), exceeding the world energy demand by a factor of more than 10,000 [2,5,7]. Hence, there is great potential in converting the sun's energy into electricity or energy rich materials, the so-called solar fuels (e.g., hydrogen, formic acid or methanol) [3,6,8].

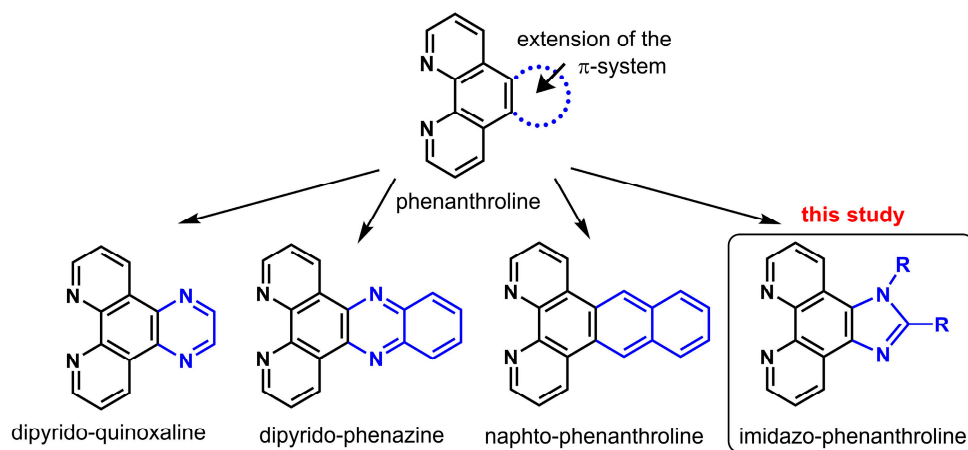
The capture and storage of sun light requires the design of efficient and inexpensive photosensitizers for light harvesting. Moreover, an ideal photosensitizer should possess a strong absorption capability in a broad range of the visible region, long-lived excited states, a reversible electrochemical behavior and high stability under ambient conditions [9–12]. In this respect, copper compounds are an attractive alternative to more traditional complexes based on precious metals like Ru(II), Re(I) or Ir(III) [9,12–14]. So far, homoleptic Cu(I) photosensitizers (CuPS) of the type $[\text{Cu}(\text{N}^{\wedge}\text{N})_2]^+$ (with $\text{N}^{\wedge}\text{N}$ = diimine ligand) are already being used in a wide range of applications such as organic light-emitting diodes (OLEDs), light-emitting electrochemical cells (LECs) or dye-sensitized solar cells (DSSCs) [13,15–18].

Due to its d^{10} configuration, the ground state geometry of Cu(I) complexes favors a (distorted) tetrahedral arrangement of the ligands around the copper center in order to minimize electrostatic repulsion [14,19]. Upon light excitation, a metal-to-ligand charge transfer (MLCT) transition from the 3d orbital of Cu(I) to the π^* -orbital of the surrounding diimine ligand takes place [14,19]. This is followed by a geometrical reorganization to a more square planar structure, corresponding to the d^9 configuration of the Cu(II) center [20,21]. Unfortunately, in this flattened state, geometry copper bisdiimine complexes are prone to exciplex quenching, causing short excited state lifetimes and limiting their applicability in solar-energy conversion schemes [9,14,15,22].

In this context, heteroleptic Cu(I) complexes of the general scheme $[(\text{P}^{\wedge}\text{P})\text{Cu}(\text{N}^{\wedge}\text{N})]^+$, containing a diimine $\text{N}^{\wedge}\text{N}$ and a bulky $\text{P}^{\wedge}\text{P}$ diphosphine ligand, are of particular interest. These heteroleptic CuPS are often characterized by long-lived triplet excited states, high quantum yields and largely tunable redox properties [12,14,15,23,24]. It was found that bulky and rigid diphosphines such as xantphos (xant) efficiently protect the copper center against nucleophilic attack and prevent undesired exciplex quenching [14,25,26]. As a major drawback these heteroleptic diimine–diphosphine Cu(I) complexes often suffer from a limited absorption capability in the visible region and lower MLCT extinction coefficients compared to advanced Ru(II) or Ir(III) photosensitizers [12,14,27].

Nevertheless, the inherent structural variety of the underlying diimine ligands allows us to adjust the photophysical and electrochemical properties in a broad range. One option to increase the extinction coefficients and to redshift the absorption is to extend the π -system of the diimine ligand [27–29]. For this reason, in previous works different dipyrido[3,2-f:2',3'-h]-quinoxaline, dipyrido[3,2-a:2',3'-c]-phenazine or naphtho[2,3-f][4,5]phenanthroline type ligands were employed (Scheme 1) [30–34]. There, either pyrazine or benzene rings were fused onto the 1,10-phenanthroline (phen) moiety in order to extend the aromatic π -system (Scheme 1). However, to the best of our knowledge heteroleptic Cu(I) complexes of the type $[(\text{xant})\text{Cu}(\text{N}^{\wedge}\text{N})]^+$ containing imidazo-phenanthroline ligands have not been reported so far. The addition of an imidazole unit represents an interesting option, as this 5-membered heteroaromatic compound is known to be π -electron rich.

Therefore, the present study deals with the synthesis and characterization of a systematic series of imidazo-phenanthroline ligands and their respective Cu(I) complexes. Starting from the 2-(4-bromophenyl)-1-phenyl-1*H*-imidazo-[4,5-*f*][1,10]phenanthroline ligand (**L2**) two novel ligands were prepared by Suzuki cross-coupling reactions (Figure 1). Subsequently, all compounds were completely analyzed by mass spectrometry (MS), NMR, UV/vis and emission spectroscopy as well as cyclic voltammetry. Moreover, the two solid-state structures of the heteroleptic Cu(I) complexes **C1** and **C2** with the general formula $[(\text{xant})\text{Cu}(\text{N}^{\wedge}\text{N})](\text{PF}_6)$ ($\text{N}^{\wedge}\text{N}$ = **L1** or **L2**) are also reported. Finally, this elucidation of structural and spectroscopic features allowed for the identification of structure-property relationships, which are useful for the future design of such heteroleptic Cu(I) photosensitizers.



Scheme 1. Different options for extending the aromatic π -system in the backbone of 1,10-phenanthroline.

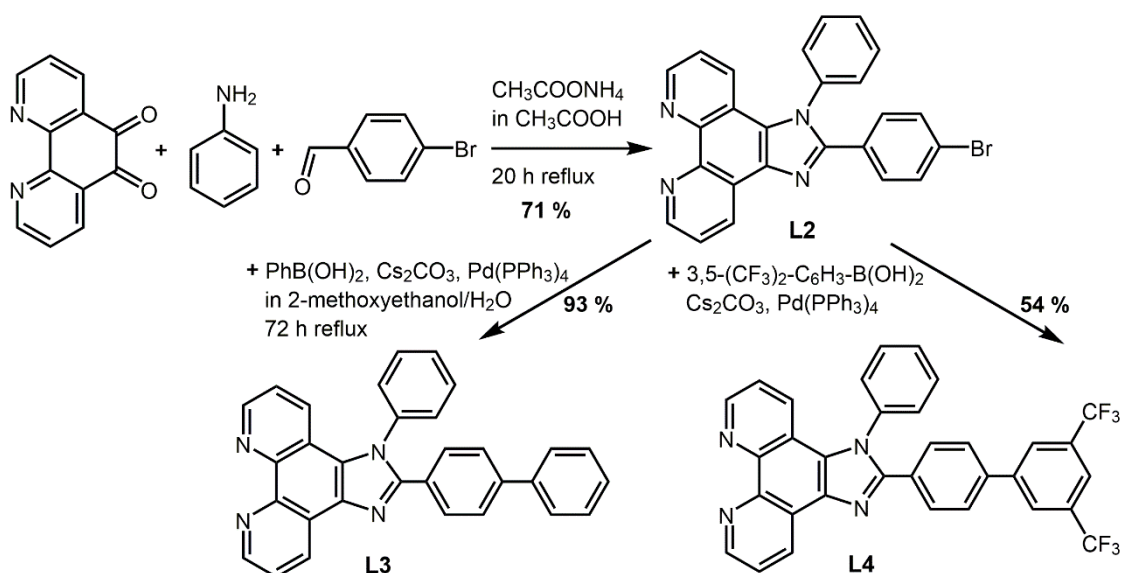


Figure 1. Synthesis details, reaction conditions, yields and labeling of the ligands L2–L4.

2. Results and Discussion

2.1. Synthesis and Structural Characterization

Initially, the imidazo-phenanthroline ligands **L1** and **L2** were prepared by a convenient condensation reaction of 1,10-phenanthroline-5,6-dione with aniline and benzaldehyde (**L1**) or 4-bromo-benzaldehyde (**L2**) in the presence of ammonium acetate (Figure 1) [35,36]. This multicomponent approach enabled the straightforward synthesis of both ligands by only one step in high yields (**L1**: 75% and **L2**: 71%). To further extend the π -system in the back of this imidazo-phenanthroline ligands, the Suzuki cross-coupling reaction was used (Figure 1). On the one hand, **L2** was reacted with phenylboronic acid using $\text{Pd}(\text{PPh}_3)_4$ as catalysts and Cs_2CO_3 as base to yield **L3** in 93%. On the other hand, **L2** was treated with 3,5-bis(trifluoromethyl)phenylboronic acid under the same conditions (2.5 mol % $\text{Pd}(\text{PPh}_3)_4$, in 2-methoxyethanol/water (9/1), 72 h reflux) to obtain **L4** in 54%. Both ligands **L3** and **L4** were purified either by column chromatography (**L3** with dichloromethane/methanol, 9/1) or recrystallization (**L4** with dichloromethane/*n*-hexane). As a result, two novel imidazo-phenanthroline ligands were obtained, containing an additional biphenyl unit in the case of **L3** and two strongly electron withdrawing trifluoromethyl groups in the case of **L4**. Hence,

the imidazo-phenanthroline ligand **L2** serves as an ideal platform for a series of gradually extended diimine ligands.

Next, the heteroleptic Cu(I) complexes **C1–C4** (Figure 2) were synthesized starting from the $[\text{Cu}(\text{ACN})_4]\text{PF}_6$ (ACN = acetonitrile) precursor via an established one-pot two-step procedure [26,31]. In the absence of oxygen (N_2 atmosphere) the xantphos (xant) ligand is introduced first, forming the $[(\text{xant})\text{Cu}(\text{ACN})_2]^+$ intermediate, followed by a quick substitution of the remaining acetonitrile ligands by the respective diimine ligand. After purification the Cu(I) compounds were obtained as yellow to slightly orange solids (Figure 2 right) in varying yields of **C1**: 76%, **C2**: 68%, **C3**: 66% and **C4**: 41% (for further details see the Experimental Section below).

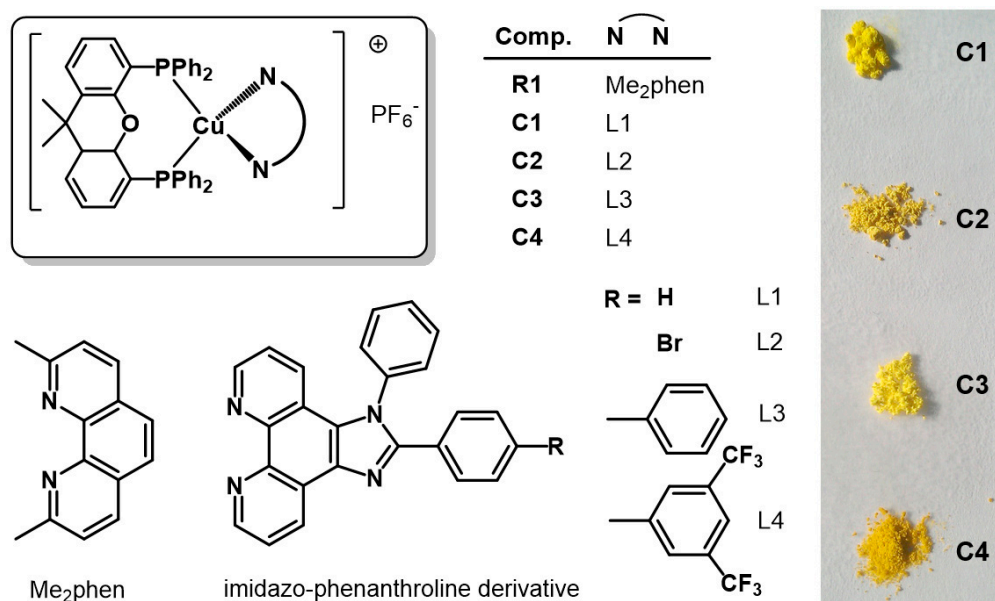


Figure 2. Left: Overview of the imidazo-phenanthroline type ligands **L1–L4** and their corresponding heteroleptic Cu(I) complexes **C1–C4** as well as the reference compound **R1** investigated in this study. Right: Photograph of the complexes **C1–C4** showing their different colors in the solid state.

All complexes were characterized by various NMR methods (^1H , ^{31}P and ^{13}C NMR), mass spectrometry (using electrospray ionization), elemental analysis and where possible also by single crystal X-ray analysis. High-resolution mass spectra with matching isotopic patterns (see Supplementary Material Figures S5 and S6) confirmed the composition of all complexes. The $[\text{M}-1\text{PF}_6]^+$ peak was found as the most prominent peak in each case. The different NMR measurements (see Supplementary Material Figures S1–S4) are all in agreement with the proposed structures. Notably, there is almost no change in the $^{31}\text{P}\{^1\text{H}\}$ chemical shifts of **C1** (–12.57 ppm), **C2** (–12.52 ppm), **C3** (–12.53 ppm) and **C4** (–12.60 ppm) (Figure 3). Furthermore, these shifts are very similar to the one of the reference compound **R1** (–13.44 ppm) with the much smaller 2,9-dimethyl-10-phenanthroline (Me_2phen) ligand. This indicates that the structure around the Cu(I) moiety and the coordination of the xantphos ligand is almost unaffected by the variation of the phenanthroline backbone. This observation is in agreement with previous studies dealing with dipyrido-quinoxaline or dipyrido-phenazine type ligands for the extension of the aromatic π -system of the phenanthroline moiety [32,33].

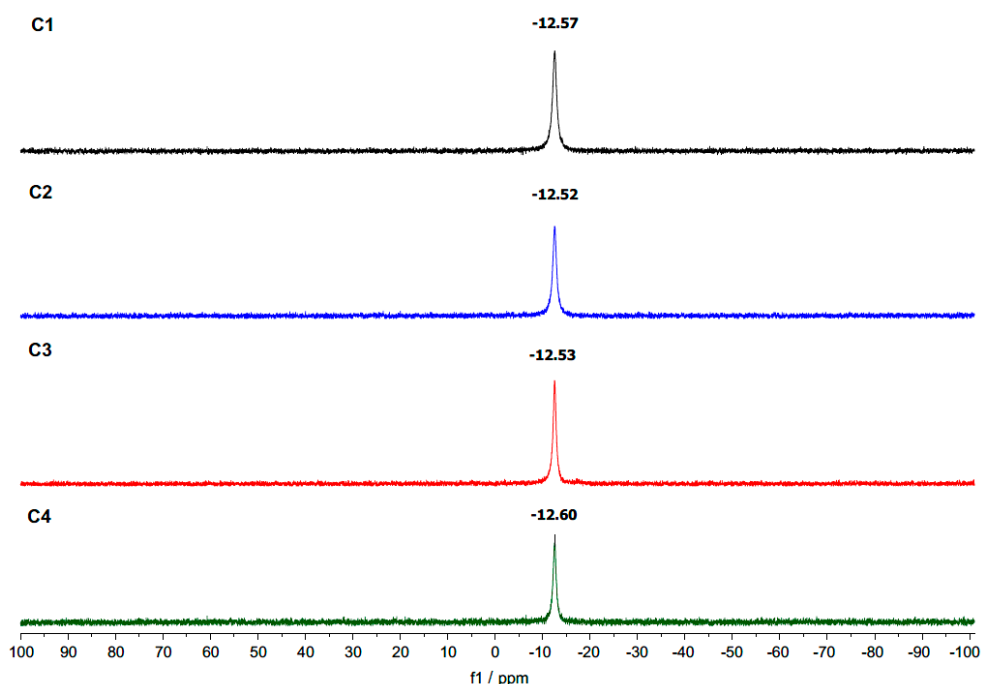


Figure 3. Comparison of the $^{31}\text{P}\{^1\text{H}\}$ -NMR spectra (at 162 MHz, in CD_3CN) of the heteroleptic copper complexes **C1**–**C4** (from top to bottom).

The proposed structures of the present heteroleptic Cu(I) complexes were further supported by X-ray crystallography. Suitable single crystals of **C1** and **C2** (both monoclinic crystal system) were received by evaporation of a saturated DCM/ethanol/*n*-hexane or a DCM/pentane solution (DCM = dichloromethane), respectively. X-ray analysis (Figure 4) confirmed the characteristic distorted tetrahedral geometry for these kinds of heteroleptic Cu(I) complexes [14,26,32,37]. This distortion is caused by the different size and bite angle of the diimine (e.g., for **C2** N1–Cu–N2: $80.48(17)^\circ$) compared to the xantphos ligand (e.g., P1–Cu–P2: $113.21(6)^\circ$, Table 1). Furthermore, both solid-state structures exhibit a twisted conformation of the two phenyl rings of **L1** and **L2**, while the imidazo-phenanthroline moiety itself is planar. The comparison of selected bond lengths and angles of **C1**, **C2** and **R2** does not show any major differences (Table 1), e.g., Cu–N1 for **C1**: 206.6(7), **C2**: 209.0(4) and **R1**: 208.4(3) pm or N1–Cu–N2 for **C1**: $79.7(3)$, **C2**: $80.48(17)$ and **R1**: $80.53(13)^\circ$. This indicates that the different ligand backbones only have a minor influence on the central structure around the copper center.

From the packing diagram of **C2** (Figure 4c), it becomes obvious that there are no π – π interactions in between the imidazo-phenanthroline ligands of neighboring complexes in the solid state. This is mainly caused by the 4-bromo-1-phenyl substituent, which is pushed in between the ligands. This observation is in contrast to **C1** (see Supplementary Material Figure S8) and to other heteroleptic Cu(I) complexes containing structurally related diimine ligands with an extended π -system. For instance, in $[(\text{xant})\text{Cu}(\text{dppz})]\text{PF}_6$ (dppz = dipyridophenazine) a pairwise stacking of the planar dppz moiety is present in the solid state [33]. Likewise, in complex **C1** a pairwise stacking is found, which is caused by π – π interactions between two phenyl rings of **L1** of adjacent complexes.

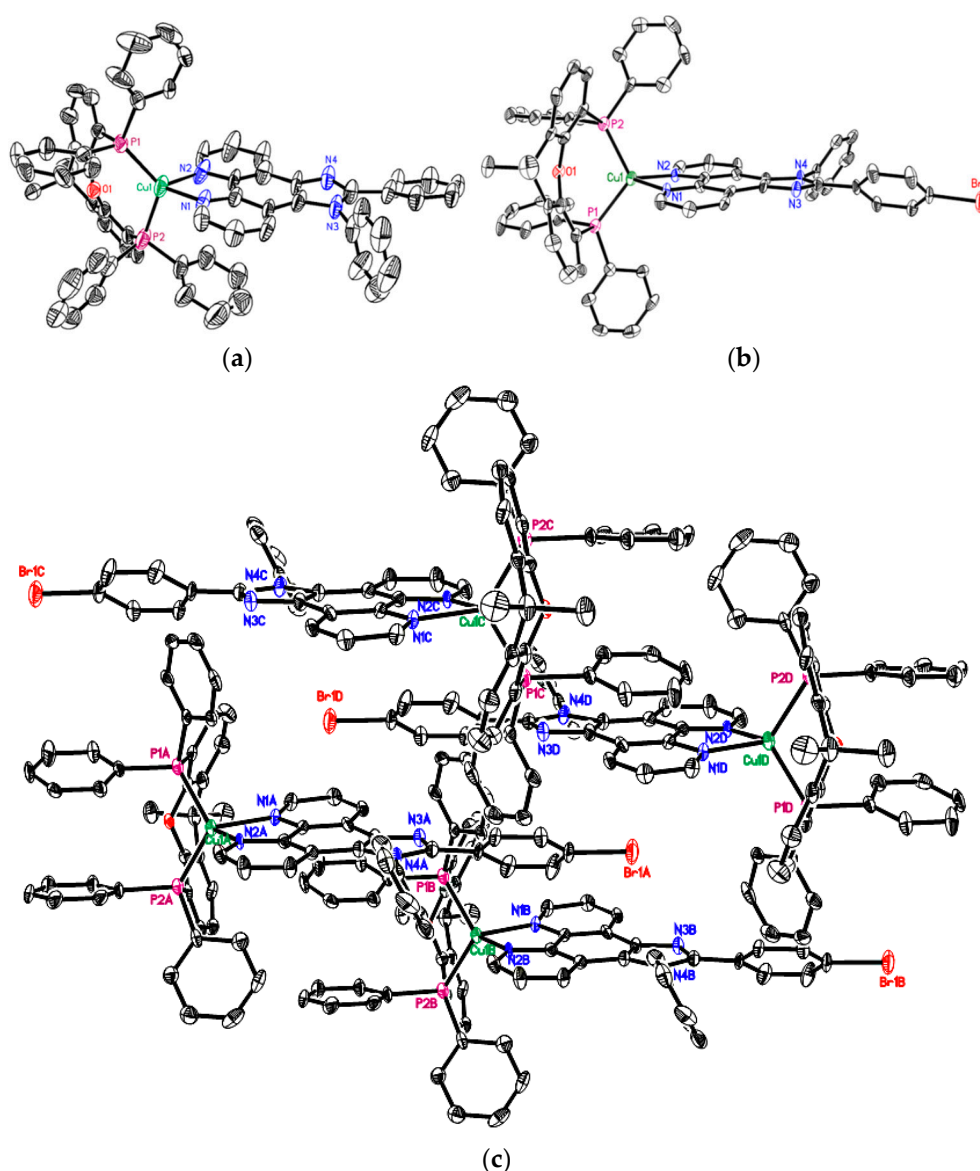


Figure 4. Solid-state structures (ORTEP representation) of (a) complex **C1** and (b) complex **C2**. (c) Packing situation of **C2** in its unit cell. The thermal ellipsoids are drawn at a probability level of 50%. Hydrogen atoms, counter anions and solvent molecules are omitted for clarity.

Table 1. Selected crystallographic bond lengths (pm) and angles ($^{\circ}$) of the complexes **C1**, **C2** and **R1**.

	C1	C2	R1 ^a
Cu–N1 [pm]	206.6(7)	209.0(4)	208.4(3)
Cu–N2 [pm]	201.6(9)	204.6(4)	211.2(3)
Cu–P1 [pm]	222.9(2)	224.14(17)	226.26(11)
Cu–P2 [pm]	227.5(3)	227.23(16)	228.63(13)
N1–Cu–N2 [$^{\circ}$]	79.7(3)	80.48(17)	80.53(13)
P1–Cu–P2 [$^{\circ}$]	118.75(8)	113.21(6)	112.93(4)
N1–Cu–P1 [$^{\circ}$]	101.8(2)	104.81(12)	108.77(9)
N1–Cu–P2 [$^{\circ}$]	127.1(2)	118.88(12)	120.33(9)
N2–Cu–P1 [$^{\circ}$]	115.3(2)	125.26(13)	120.33(9)
N2–Cu–P2 [$^{\circ}$]	106.8(2)	110.45(12)	118.59(9)

^a Data was taken from reference [32] for comparison.

2.2. Electrochemical and Photophysical Studies

The electrochemical properties of the complexes **C1–C4** were studied by cyclic voltammetry in acetonitrile solution (Figure 5, Table 2). The respective cyclic voltammograms (CVs) of **C1** and **C4** contain a fully reversible reduction wave, while the reduction waves of **C2** and **C3** are quasi-reversible at a scan rate of 100 mV/s. With faster scan rates these reduction waves become reversible (Figure 5d,e). This indicates that the singly reduced species of **C2** and **C3** are highly reactive and do already start to react further, before they are reoxidized. Therefore, this behavior can be suppressed by faster scan rates.

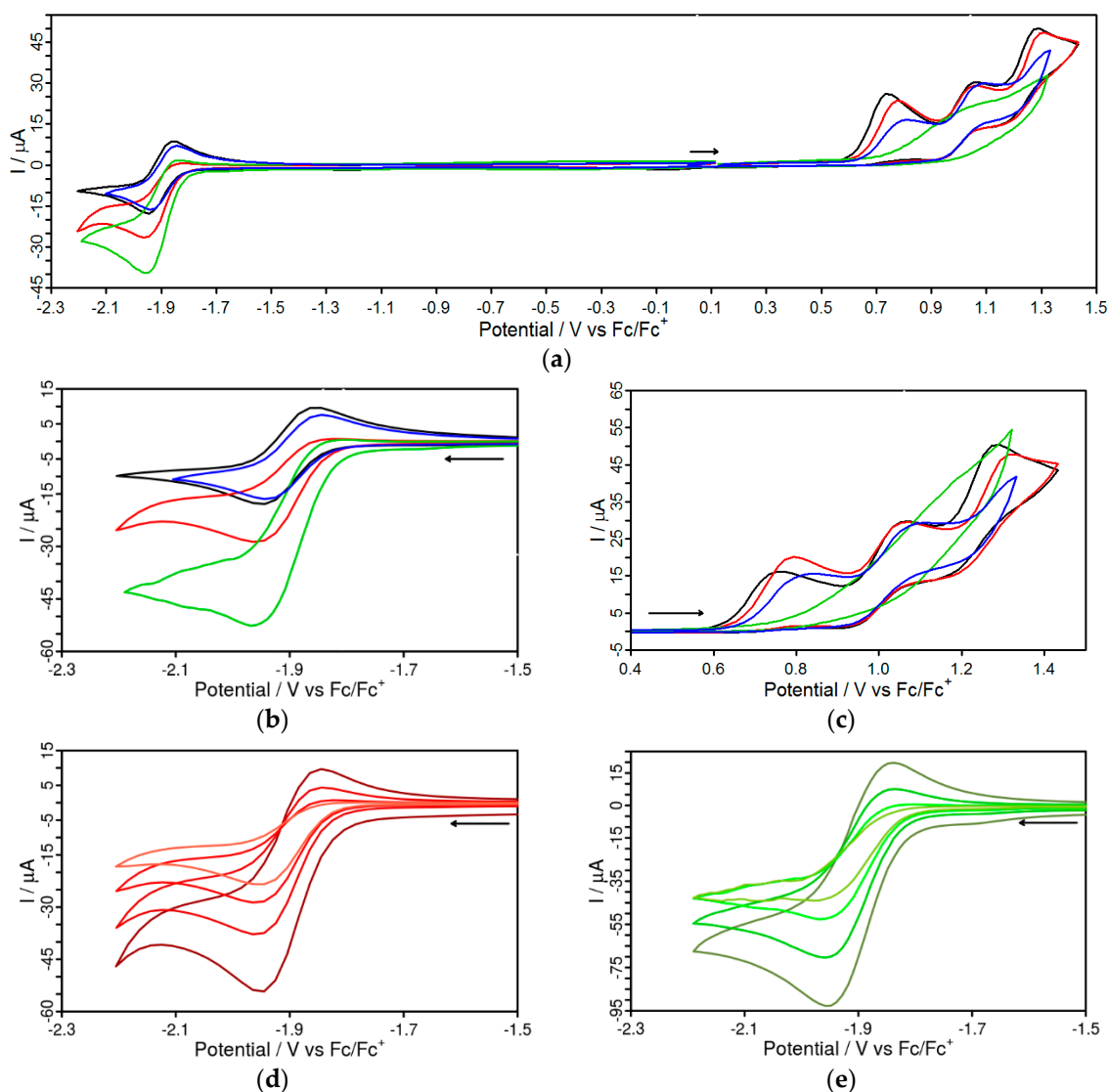


Figure 5. Cyclic voltammograms of **C1** (black), **C2** (red), **C3** (green) and **C4** (blue) in acetonitrile solution using TBAPF₆ (0.1 M) as supporting electrolyte. All measurements, if not stated otherwise, were conducted with a scan rate of 100 mV/s. The arrow illustrates the initial scan direction. In (a) the full scan is given, while in (b) the reduction waves and in (c) the oxidation waves were measured separately. In (d) the reduction waves of **C2** and in (e) of **C3** are shown with different scan rates of 500 mV/s, 250 mV/s, 100 mV/s, 50 mV/s (for **C2** from dark red to light red and **C3** from dark green to light green).

Table 2. Summary of the photophysical and electrochemical properties of the complexes **C1–C4** and their respective ligands **L1–L4**. The UV/vis absorption of the complexes was determined in aerated acetonitrile (ACN), while the ligands were measured in aerated dichloromethane (DCM) due to solubility issues. Emission of the complexes ($\lambda_{\text{exc}} = 400 \text{ nm}$) was detected at room temperature in acetonitrile in the absence of oxygen and of the ligands ($\lambda_{\text{exc}} = 355 \text{ nm}$) in dichloromethane under the same conditions. For the emission lifetime measurements all samples were excited at 355 nm. Redox potentials of the complexes **C1–C4** were measured in deaerated acetonitrile and of the ligands **L1–L4** in deaerated dichloromethane with 0.1 M TBAPF₆ as supporting electrolyte vs. Fc/Fc⁺.

Comp.	$\lambda_{\text{max,abs}} [\text{nm}]$ ($\epsilon [10^3 \text{ M}^{-1} \text{ cm}^{-1}]$)	$\lambda_{\text{max,em}} [\text{nm}]$ ACN	$\lambda_{\text{max,em}} [\text{nm}]$ (LC) DCM	$\lambda_{\text{max,em}} [\text{nm}]$ (MLCT) DCM	$\lambda_{\text{max,em}} [\text{nm}]$ solid	$\tau [\text{ns}]$ solid	$E_{1/2 \text{ red}} [\text{V}]$	$E_{\text{ox1}} [\text{V}]^{\text{a}}$	$E_{\text{ox2}} [\text{V}]^{\text{a}}$
R1	378 (3.1) ^b	564 ^b			518 ^c	167, 1702 ^c	−2.10 ^b	0.82 ^b	-
C1	403 (6.00)	474	454	618	573	14, 286	−2.01	0.73	0.99
C2	400 (5.73)	457	452	613	574	12, 426	−1.98	0.85	1.11
C3	403 (8.64)	474	454	614	564	15, 438	−1.97	0.55	0.65
C4	401 (6.49)	478	454	611	576	20, 438	−1.97	0.77	1.02
L1	274 (59.05)		408				-	1.19	1.52
L2	277 (64.77)		409				-	1.25	1.46
L3	283 (41.11)		413				-	1.23	1.46
L4	284 (40.02)		410				-	1.22	1.43

^a Irreversible. ^b Taken from [32]. ^c First reported here.

In each complex the reduction wave corresponds to an one electron reduction, already proven to be the reduction of the diimine ligand forming the $[(P^*P)Cu^I(N^*N^-)]$ species [14,38,39]. Interestingly, the reduction potentials of all complexes are very similar and occur in the range between -2.01 V (C1) to -1.97 V (C4). Hence, the different substituents at the imidazo-phenanthroline backbone only have a minor influence, indicating that the imidazo moiety is electronically decoupled from the phenanthroline sphere. This behavior was also observed for related Ru(II) complexes [40,41]. In contrast, a cathodic shift > 100 mV takes place compared to R1 ($E_{red} = -2.10$ V) due to the overall extended π -system of the imidazo-phenanthroline ligands. This significant shift does not appear for Ru(II) complexes containing such imidazole ligands that show a similar behavior to their Ru(II) phenanthroline complexes instead [41].

The oxidation waves are irreversible and attributed to the oxidation of the phosphine ligand, resulting in a dissociation of the P–Cu bond. This behavior is characteristic for heteroleptic Cu(I) complexes containing a xantphos ligand [14,26,32,38]. The oxidation potentials of the complexes differ with the different diimine ligands. For instance, the first oxidation takes place in the range from $E_{ox1} = 0.55$ V (C3) to 0.85 V (C2).

All copper complexes C1–C4 possess strong absorption bands in the UV region in acetonitrile solution (Figure 6c), which can be assigned to ligand centered absorption of the imidazo-phenanthroline ligand. They also show strong metal-to-ligand charge transfer (MLCT) transition bands around 400 nm. These bands are more than 20 nm (~ 1316 cm^{-1}) bathochromically shifted compared to the reference complex R1 ($\lambda_{max,abs} = 378$ nm, Table 2) without any imidazo moiety [32]. This phenomenon is also observed for related Ru(II) complexes, although it is less pronounced there (~ 6 nm) [28,42]. Moreover, the absorptivity of the novel complexes C1–C4 is significantly increased, which illustrates the impact of the extended π -system. The highest molar extinction coefficients for the respective MLCT bands were found for C3 (8.6×10^3 $M^{-1} cm^{-1}$) and C4 (6.5×10^3 $M^{-1} cm^{-1}$). Furthermore, the UV/vis absorption spectrum of complex C4 has an additional shoulder around 350 nm. This shoulder can be attributed to additional π - π^* charge transfer transitions in the extended π -system [32,43]. This assignment is supported by the absorption spectra of the uncoordinated ligands L3 and L4 (Figure 6a), which also exhibit an additional shoulder at 350 nm.

The emission spectra of the Cu(I) complexes C1–C4 were measured in acetonitrile (Figure 6d) and in dichloromethane (Figure 6e) solution under an argon atmosphere, because the emission is quenched in the presence of oxygen. In acetonitrile all complexes show weak emission bands around 475 nm (Figure 6d) with quantum yields of approximately 0.003. For comparison, the emission of the corresponding ligands L1–L4 was also determined, but solely in dichloromethane due to solubility issues. Under these conditions the ligands exhibit intense emissions of around 410 nm (Figure 6b). Hence, the emission maxima of the complexes C1–C4 are redshifted compared to the pure ligands L1–L4. This means that the emission properties of the Cu(I) complexes are not caused by a potential contamination with the respective imidazo-phenanthroline ligand or a dissociation reaction in solution.

It is more likely that the weak emission of this Cu(I) complexes is attributed to ligand centered processes, because the energy of the detected emission is too high to be initiated by a triplet excited state with MLCT character. Furthermore, in dichloromethane these emission bands around 475 nm are negligible, because their intensity is only in the order of magnitude of the Raman scattering (i.e., in Figure 6e the sharp peaks belong to the Raman bands of the solvent). Additionally, in dichloromethane an emission band around 615 nm originating from a 3MLCT state appears for C1–C4 (Figure 6e), which is a typical wavelength range for the emission of such heteroleptic Cu(I) complexes [14,15,44]. In contrast, this low energy emission is not present in acetonitrile and seems to be quenched there.

Finally, also the solid-state emission was measured for the powdered samples at room temperature, where C1, C2 and C4 show a strong emission around 575 nm (Figure 6f). The emission band of C3 is comparably weaker, but shifted to higher energies with a maximum at 564 nm. Furthermore, the observed emission maxima are bathochromically shifted (~ 40 nm) compared to structurally related heteroleptic Cu(I) complexes, where the solid-state emission was strongly affected by the molecular

structure of the individual diimine ligand [45]. These $^3\text{MLCT}$ -emission-bands are rigidochromically blueshifted compared to the $^3\text{MLCT}$ -bands measured in dichloromethane.

The respective emission lifetimes of the solid samples are in the nanosecond range (Table 2) with a maximum of 438 ns for **C3** and **C4**. The maximum emission lifetimes of **C2–C4** are very similar to each other and only the lifetime of **C1** is shorter (286 ns). In contrast, the solid-state emission lifetime of the reference complex **R1** (up to 1.7 μs) is much longer. The observed emission lifetimes are all two exponential, which is in accordance to related heteroleptic copper complexes containing an imidazo-phenanthroline moiety [45].

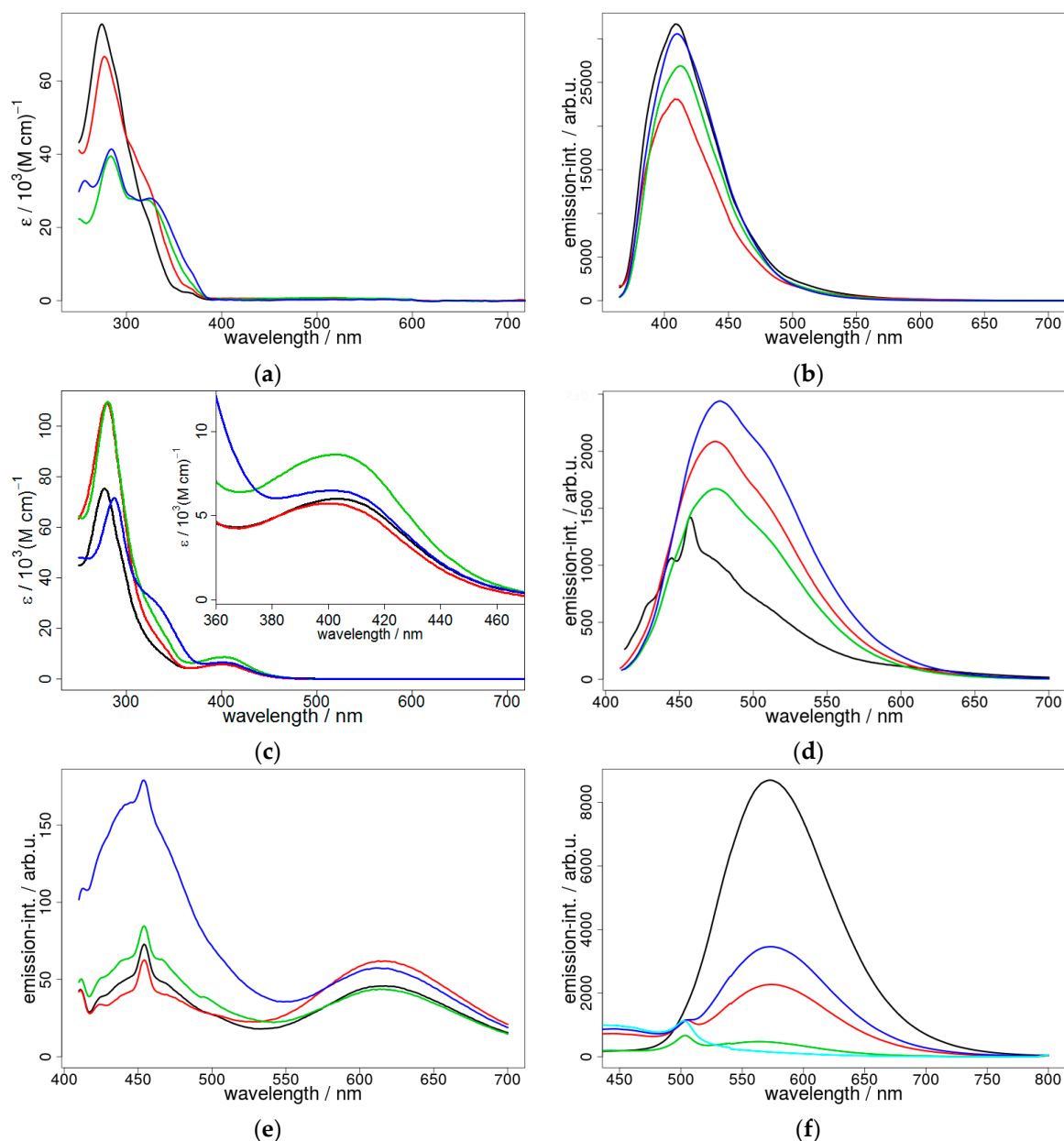


Figure 6. Absorption and emission spectra of the ligands **L1** (black), **L2** (red), **L3** (green) and **L4** (blue) (a,b) in dichloromethane and of the complexes **C1** (black), **C2** (red), **C3** (green) and **C4** (blue) (c,d) in acetonitrile solution. In panel (e) the emission spectra of **C1–C4** (all measured with an optical density of 0.1 at $\lambda_{\text{exc}} = 400$ nm) are also presented in dichloromethane solution for comparison. Emission spectra were measured at room temperature under argon atmosphere. The emission of the solid samples **C1–C4** are depicted in panel (f). The light blue line represents the emission of the blank test (only the sample holder without any sample).

3. Experimental Section

3.1. Materials and Methods

NMR: NMR spectra were measured at 298 K with different Bruker Avance spectrometers (Bruker, Rheinfelden, Germany) operating at Larmor frequencies of 400 MHz, 500 MHz or 700 MHz (^1H) and 101 MHz, 126 MHz or 176 MHz (^{13}C) and 162 MHz (^{31}P). The resulting NMR spectra are processed with Bruker TopSpin software (version 3.2). The chemical shifts δ are listed in ppm. ^1H - and ^{13}C -NMR shifts are referenced according to the applied deuterated solvent as internal standard [46]. $^{31}\text{P}\{^1\text{H}\}$ -NMR shifts are proton decoupled and given relatively to H_3PO_4 (85%, $\delta = 0$ ppm) as an external reference. Coupling constants J are presented as absolute values in Hz, without considering the kind of the coupling. For characterizing the multiplicity of the NMR signals the following abbreviations are used: s = singlet, d = doublet, t = triplet, q = quartet, m = multiplet and dd = doublet of doublets.

ESI-MS: Mass spectrometric measurements were performed by the analytical service of the Institute for Organic Chemistry (IOC) at the University of Stuttgart. Electrospray ionization (ESI) spectra were measured using a Bruker Daltonics micrOTOF-Q (Bruker, Rheinfelden, Germany). The respective values are given as m/z .

X-ray: Single crystal X-ray diffraction analyses were carried out at 130 K on a Bruker Kappa APEXII Duo diffractometer (Bruker, Rheinfelden, Germany) with graphite-monochromated $\text{Mo K}\alpha$ ($\lambda = 0.71073 \text{ \AA}$) or $\text{Cu K}\alpha$ ($\lambda = 1.54178 \text{ \AA}$) radiation by using Omega-Phi scan technique [47]. The structures were solved by direct methods using *SHELXL97* software. ORTEP molecular graphics were performed by XP software [48]. CCDC 1875532 (C1) and 1875530 (C2) contain the supplementary crystallographic data for this paper. These data can be obtained free of charge via <http://www.ccdc.cam.ac.uk/conts/retrieving.html>.

Absorption spectroscopy: Steady-state UV/vis absorption spectra were measured with a JASCO V-670 spectrophotometer (JASCO, Pfungstadt, Germany). The complexes C1–C4 and the ligands L1–L4 were dissolved in acetonitrile and in dichloromethane, respectively. Both solvents were of spectroscopic grade. All spectra were recorded in a standard 10 mm fluorescence quartz glass cuvette.

Emission spectroscopy: Steady-state emission spectra were recorded with a JASCO 25 spectrofluorometer FP-8500 (JASCO, Pfungstadt, Germany). The complexes C1–C4 and the ligands L1–L4 were dissolved in acetonitrile and in dichloromethane, respectively. All samples in solution were measured under inert conditions in a standard 10 mm fluorescence quartz glass cuvette with an optical density of approximately 0.1 at 400 nm. The solid samples were measured using a glass slide and fixed with a double-sided adhesive tape.

Time-resolved emission spectroscopy: Emission lifetime measurements were performed using a Q-switched pulsed Nd:YAG laser (Q-smart 450 mJ, Quantel laser, Les Ulis Cedex, France) with pulse durations of approx. 6 ns (repetition rate of 10 Hz). As excitation pulses the Nd:YAG output centered at 355 nm were used. The power of the pump beam was about 1.1 mJ per pulse at the sample. The emission lifetime of the samples was measured at their respective emission maxima. The emitted light was recorded using a photo multiplier tube (Hamamatsu R928P, Hamamatsu Photonics, Hamamatsu, Japan) of the LP980 spectrometer (Edinburgh Instruments, Livingston, UK).

Cyclic voltammetry: The cyclic voltammograms were carried out in acetonitrile or dichloromethane, respectively. As the supporting electrolyte 0.1 M TBAPF₆ was used. The measurements were performed with an Autolab potentiostat PGSTAT204 (Metrohm, Filderstadt, Germany) using a three-electrode configuration. As electrodes a glassy carbon disc with a 3 mm diameter stick (working), a Pt electrode (counter) and a non-aqueous Ag/Ag⁺ electrode with 0.01 M AgNO₃ in acetonitrile (reference) were utilized. As reference the ferrocene/ferrocenium (Fc/Fc⁺) couple was applied, which was added to

the solution after each measurement. Thus, all reported potentials are versus the Fc/Fc⁺ couple. All scan rates are 100 mV/s unless otherwise noted.

3.2. Synthesis and Characterization

The starting materials (e.g., [Cu(ACN)₄]PF₆, xantphos or 1,10-phenanthroline) were purchased from the commercial suppliers ABCR, Acros Organics, Fluka, Sigma-Aldrich and VWR and used without further purification. Solvents were purified and dried according to conventional procedures [49]. All Suzuki cross-coupling reactions and the preparations of the heteroleptic Cu(I) complexes were performed under nitrogen atmosphere by using standard Schlenk techniques.

The ligands 2-phenyl-1-phenyl-1*H*-imidazo-[4,5-*f*][1,10]phenanthroline (**L1**) and 2-(4-bromophenyl)-1-phenyl-1*H*-imidazo-[4,5-*f*][1,10]phenanthroline (**L2**) were synthesized according to literature matching all reported characterization [35,36].

2-([1,1'-Biphenyl]-4-yl)-1-phenyl-1*H*-imidazo[4,5-*f*][1,10]phenanthroline L3: The ligand **L3** was prepared by reacting 400 mg (0.886 mmol) **L2** with 161 mg (1.321 mmol) PhB(OH)₂ in the presence of 144 mg (0.442 mmol) Cs₂CO₃ and 26 mg (0.022 mmol) Pd(PPh₃)₄ in a mixture of 2-methoxyethanol:water (9:1) under reflux for 72 h. After cooling to room temperature, water was added and the aqueous phase was extracted with DCM. The solvent was removed in vacuo and the crude product was purified by column chromatography (DCM:MeOH, 9:1). Yield: 93% (371 mg).

¹H-NMR (CDCl₃, 400 MHz, 25 °C): δ (ppm) = 9.14–9.09 (*m*, 2H, Ar-*H*), 8.98 (*d*, 1H, *J* = 4.4, Ar-*H*), 7.70 (*dd*, 1H, *J* = 8.0, 4.4, Ar-*H*), 7.63–7.56 (*m*, 5H, Ar-*H*), 7.52–7.47 (*m*, 4H, Ar-*H*), 7.47 (*s*, 1H, Ar-*H*), 7.41–7.33 (*m*, 4H, Ar-*H*), 7.29 (*d*, 1H, *J* = 7.5, Ar-*H*), 7.24 (*dd*, 1H, *J* = 8.3, 4.3, Ar-*H*). **¹³C-NMR (CD₃CN, 101 MHz, 25 °C):** δ (ppm) = 152.0, 149.0, 147.9, 144.7, 144.2, 142.0, 140.1, 138.1, 136.3, 134.1, 130.8, 130.6, 130.4, 129.6, 128.9, 128.8, 128.7, 128.2, 127.8, 127.7, 127.0, 124.1, 123.6, 122.2, 120.0. **HRMS (ESI) *m/z*:** calculated for [M – H]⁺ [C₃₁H₂₁N₄]⁺: 449.1761; found: 449.1765.

2-(3',5'-Bis(trifluoromethyl)[1,1'-biphenyl]-4-yl)-1-phenyl-1*H*-imidazo[4,5-*f*][1,10]phenanthroline L4: The Ligand **L4** was prepared by reacting 600 mg (1.33 mmol) **L2** with 525 mg (2.04 mmol) 3,5-(CF₃)₂-C₆H₃-B(OH)₂ in the presence of 217 mg (0.67 mmol) Cs₂CO₃ and 38 mg (0.033 mmol) Pd(PPh₃)₄ in a mixture of 2-methoxyethanol:water (9:1) under reflux for 72 h. After cooling to room temperature, water was added and the aqueous phase was extracted with DCM. Upon removal of the solvent, the product began to precipitate. It was collected by filtration and washed with *n*-hexane and water. Yield: 54% (422 mg).

¹H-NMR (CDCl₃, 700 MHz, 25 °C): δ (ppm) = 9.13 (*dd*, 1H, *J* = 4.3, 1.7, Ar-*H*), 9.09 (*dd*, 1H, *J* = 8.1, 1.7, Ar-*H*), 8.99 (*dd*, 1H, *J* = 4.2, 1.5, Ar-*H*), 7.93 (*s*, 2H, Ar-*H*), 7.80 (*s*, 1H, Ar-*H*), 7.70 (*dd*, 1H, *J* = 8.0, 4.3, Ar-*H*), 7.67 (*d*, 2H, *J* = 8.4, Ar-*H*), 7.65 (*d*, 1H, *J* = 7.3, Ar-*H*), 7.64–7.61 (*m*, 2H, Ar-*H*), 7.51 (*t*, 4H, *J* = 7.2, Ar-*H*), 7.39–7.37 (*m*, 1H, Ar-*H*), 7.23 (*dd*, 1H, *J* = 8.4, 4.3, Ar-*H*). **¹³C-NMR (CD₃CN, 176 MHz, 25 °C):** δ (ppm) = 150.0, 148.2, 147.1, 144.0, 143.5, 141.2, 137.7, 136.9, 135.3, 131.3, 129.7, 129.5, 129.5, 129.4, 129.0, 127.7, 127.0, 126.1, 126.1, 123.0, 122.9, 122.5, 121.5, 121.2, 120.3, 118.8. **HRMS (ESI) *m/z*:** calculated for [M – H]⁺ [C₃₃H₁₉F₆N₄]⁺: 585.1508; found: 585.1535. **EA:** calculated for C₃₁H₂₀F₆N₄: C: 67.81, H: 3.10, N: 9.59; found: C: 67.35, H: 3.48, N: 9.41.

The heteroleptic Cu(I) complexes **C1–C4** were all prepared using a standard one-pot two-step procedure. For this purpose, one equivalent of [Cu(ACN)₄]PF₆ and one equivalent of xantphos were suspended in dry and degassed dichloromethane. Then, this reaction mixture was heated to reflux for 16 h under N₂ atmosphere. After cooling the mixture to 0 °C using an ice bath the respective imidazo-phenanthroline ligand (1 equiv.), dissolved in a small amount of DCM, was added dropwise. Afterwards, this mixture was stirred for another 2–3 h under reflux. After cooling to room temperature, the product was precipitated by the addition of *n*-hexane and allowed to stand in a freezer overnight for full precipitation. Finally, the solid was filtered off, thoroughly washed with H₂O, Et₂O and *n*-hexane, then dried *in vacuo*.

[(xant)Cu(L1)](PF₆) C1: According to the standard procedure **C1** was prepared by reacting 75 mg (0.200 mmol) [Cu(ACN)₄](PF₆) with 116 mg (0.200 mmol) Xantphos and 74 mg (0.200 mmol) **L1**. Yield: 76% (177 mg).

¹H-NMR (CD₃CN, 500 MHz, 25 °C): δ (ppm) = 9.06 (*d*, 1H, *J* = 8.2, Ar-H), 8.43 (*d*, 1H, *J* = 4.4, Ar-H), 8.27 (*d*, 1H, *J* = 4.4, Ar-H), 7.72–7.66 (*m*, 3H, Ar-H), 7.65 (*d*, 4H, *J* = 7.0, Ar-H), 7.61 (*t*, 2H, *J* = 7.6, Ph-H), 7.58–7.53 (*m*, 4H, Ar-H), 7.42 (*d*, 1H, *J* = 8.4, Ar-H), 7.38–7.33 (*m*, 1H, Ar-H), 7.30 (*t*, 2H, *J* = 7.6, Ph-H), 7.24 (*dd*, 1H, *J* = 8.5, 3.8, Ar-H), 7.18–7.08 (*m*, 6H, Ar-H), 6.98 (*t*, 8H, *J* = 7.5, Ph-H), 6.89–6.82 (*m*, 8H, Ar-H), 6.54–6.48 (*m*, 8H, Ar-H), 1.67 (*d*, 6H, *J* = 7.4, CCH₃). ¹³C-NMR (CD₃CN, 126 MHz, 25 °C): δ (ppm) = 154.7, 153.4, 147.6, 146.7, 141.4, 141.3, 137.2, 135.7, 134.1, 132.5, 131.5, 131.4, 131.3, 131.1, 130.9, 130.6, 129.8, 129.6, 129.5, 129.3, 129.2, 128.5, 128.5, 128.3, 127.6, 127.1, 125.3, 125.1, 124.9, 124.2, 121.2, 119.3, 35.9, 27.3. ³¹P-NMR (CD₃CN, 162 MHz, 25 °C): δ (ppm) = –12.6. HRMS (ESI) *m/z*: calculated for [M]⁺ [C₆₄H₄₈CuN₄OP₂]⁺: 1013.2594; found: 1013.2572. EA: calculated for C₆₄H₄₈CuF₆N₄OP₃: C: 66.29, H: 4.17, N: 4.83; found: C: 65.28, H: 4.26, N: 4.77.

Crystals suitable for X-ray analysis were obtained from a saturated DCM/ethanol/*n*-hexane solution. The following crystal Data for C₆₅H₅₀Cl₂CuF₆N₄OP₃ (M = 1244.44 g/mol) were received: monoclinic, space group P2(1)/n, *a* = 12.1254(10) Å, *b* = 13.9304(12) Å, *c* = 40.007(3) Å, α = 90°, β = 93.564(4)°, γ = 90°, *V* = 6744.6(10) Å³, *Z* = 4, *T* = 130(2) K, *D*_{calc} = 1.226 mg/m³, 39834 reflections measured (1.548° ≤ 2θ ≤ 25.473°), 12284 unique (Rint = 0.0732) which were used in all calculations. The final R1 was 0.1232 (*I* > 2σ(*I*)) and wR² was 0.2824 (all data).

[(xant)Cu(L2)](PF₆) C2: According to the standard procedure **C2** was prepared by reacting 83 mg (0.223 mmol) [Cu(ACN)₄](PF₆) with 129 mg (0.223 mmol) Xantphos and 100 mg (0.223 mmol) **L2**. Yield: 68% (184 mg).

¹H-NMR (CD₃CN, 500 MHz, 25 °C): δ (ppm) = 9.04 (*d*, 1H, *J* = 8.0, Ar-H), 8.44 (*d*, 1H, *J* = 4.0, Ar-H), 8.28 (*d*, 1H, *J* = 4.1, Ar-H), 7.72–7.65 (*m*, 4H, Ar-H), 7.62 (*t*, 2H, *J* = 7.4, Ar-H), 7.58–7.52 (*m*, 2H, Ar-H), 7.48–7.39 (*m*, 5H, Ar-H), 7.24 (*dd*, 1H, *J* = 8.4, 4.6, Ar-H), 7.17–7.09 (*m*, 6H, Ar-H), 6.98 (*t*, 8H, *J* = 7.3, Ph-H), 6.90–6.81 (*m*, 8H, Ar-H), 6.56–6.48 (*m*, 2H, Ar-H), 1.66 (*d*, 6H, *J* = 7.0, CCH₃). ¹³C-NMR (CD₃CN, 126 MHz, 25 °C): δ (ppm) = 154.6, 152.0, 147.5, 146.7, 141.4, 141.2, 136.8, 135.5, 134.0, 132.4, 131.3, 131.1, 131.0, 130.7, 130.7, 130.6, 129.7, 129.6, 129.1, 128.5, 128.4, 128.3, 127.5, 127.1, 125.2, 124.8, 124.8, 124.1, 123.5, 121.0, 119.1, 35.7, 27.2. ³¹P-NMR (CD₃CN, 162 MHz, 25 °C): δ (ppm) = –12.5. HRMS (ESI) *m/z*: calculated for [M]⁺ [C₆₄H₄₇BrCuN₄OP₂]⁺: 1093.1692; found: 1093.1662. EA: calculated for C₆₄H₄₇BrCuF₆N₄OP₃: C: 62.07, H: 3.83, N: 4.52; found: C: 57.33, H: 3.88, N: 4.06.

Crystals suitable for X-ray analysis were obtained from a saturated DCM/pentane solution. The following crystal Data for C₆₅H₄₉BrCl₂CuF₆N₄OP₃ (M = 1323.34 g/mol) were received: monoclinic, space group P 21/c, *a* = 9.8687(8) Å, *b* = 27.521(2) Å, *c* = 21.7494(17) Å, α = 90°, β = 95.369(2)°, γ = 90°, *V* = 5881.2(8) Å³, *Z* = 4, *T* = 130(2) K, *D*_{calc} = 1.495 mg/m³, 40422 reflections measured (1.48° ≤ 2θ ≤ 25.07°), 10384 unique (Rint = 0.1441) which were used in all calculations. The final R1 was 0.0700 (*I* > 2σ(*I*)) and wR² was 0.1047 (all data).

[(xant)Cu(L3)](PF₆) C3: According to the standard procedure **C3** was prepared by reacting 83 mg (0.223 mmol) [Cu(ACN)₄](PF₆) with 129 mg (0.223 mmol) Xantphos and 74 mg (0.223 mmol) **L3**. Yield: 66% (177 mg).

¹H-NMR (CD₃CN, 700 MHz, 25 °C): δ (ppm) = 9.18 (*d*, 1H, *J* = 7.9, Ar-H), 8.56 (*d*, 1H, *J* = 4.1, Ar-H), 8.39 (*d*, 1H, *J* = 4.2, Ar-H), 9.82 (*d*, 2H, *J* = 7.9, Ar-H), 7.81–7.78 (*m*, 2H, Ar-H), 7.76–7.73 (*m*, 4H, Ar-H), 7.69 (*d*, 2H, *J* = 7.5, Ar-H), 7.63 (*d*, 4H, *J* = 8.0, Ar-H), 7.51 (*d*, 1H, *J* = 8.5, Ar-H), 7.47 (*t*, 2H, *J* = 7.5, Ar-H), 7.41 (*t*, 1H, *J* = 7.4, Ar-H), 7.34 (*dd*, 1H, *J* = 8.5, 4.6, Ar-H), 7.28–7.25 (*m*, 4H, Ar-H), 7.23 (*t*, 2H, *J* = 7.7, Ar-H), 7.10 (*t*, 8H, *J* = 7.5, Ph-H), 7.01–6.96 (*m*, 8H, Ar-H), 6.65–6.62 (*m*, 2H, Ar-H), 1.79 (*d*, 6H, *J* = 9.7, CCH₃). ¹³C-NMR (CD₃CN, 176 MHz, 25 °C): δ (ppm) = 155.4, 153.6, 148.4, 147.4, 142.5, 142.2, 142.0, 140.0, 138.0, 136.5, 134.9, 133.3, 132.2, 132.0, 131.6, 131.5, 131.4, 130.6, 130.5, 130.3,

130.0, 129.6, 129.3, 129.2, 128.6, 128.4, 127.9, 127.4, 127.4, 126.1, 125.8, 125.7, 125.0, 121.9, 120.0, 36.6, 28.1. ³¹P-NMR (CD₃CN, 162 MHz, 25 °C): δ (ppm) = −12.5. HRMS (ESI) *m/z*: calculated for [M]⁺ [C₇₀H₅₂CuN₄OP₂]⁺: 1089.2907; found: 1089.2884. EA: calculated for C₇₀H₅₂CuF₆N₄OP₃: C: 68.04, H: 4.24, N: 4.53; found: C: 67.41, H: 4.63, N: 4.02.

[(xant)Cu(L4)](PF₆) C4: According to the standard procedure C4 was prepared by reacting 64 mg (0.171 mmol) [Cu(ACN)₄]⁺PF₆[−] with 99 mg (0.171 mmol) Xantphos and 100 mg (0.171 mmol) L4. Yield: 41% (177 mg).

¹H-NMR (CD₃CN, 400 MHz, 25 °C): δ (ppm) = 9.18 (*d*, 1H, *J* = 8.0, Ar-*H*), 8.54 (*d*, 1H, *J* = 4.3, Ar-*H*), 8.38 (*d*, 1H, *J* = 4.4, Ar-*H*), 8.21 (*s*, 2H, Ar-*H*), 8.03 (*s*, 1H, Ar-*H*), 7.83–7.69 (*m*, 12H, Ar-*H*), 7.52 (*d*, 1H, *J* = 8.4, Ar-*H*), 7.35 (*dd*, 1H, *J* = 7.6, 4.7, Ar-*H*), 7.28–7.19 (*m*, 6H, Ar-*H*), 7.08 (*t*, 8H, *J* = 7.4, Ph-*H*), 6.99–6.92 (*m*, 8H, Ar-*H*), 6.65–6.59 (*m*, 2H, Ar-*H*), 1.76 (*d*, 6H, *J* = 5.3, CCH₃). ¹³C-NMR (CD₃CN, 101 MHz, 25 °C): δ (ppm) = 155.5, 153.3, 148.5, 147.6, 142.6, 142.3, 142.1, 139.5, 137.9, 136.6, 134.9, 133.3, 132.4, 132.2, 132.1, 132.0, 131.9, 131.8, 131.7, 131.5, 130.8, 130.6, 130.1, 129.3, 128.4, 128.2, 128.1, 126.1, 125.8, 125.7, 125.5, 125.0, 122.8, 122.1, 121.9, 120.0, 36.7, 28.1. ³¹P-NMR (CD₃CN, 162 MHz, 25 °C): δ (ppm) = −12.6. HRMS (ESI) *m/z*: calculated for [M]⁺ [C₇₂H₅₀CuF₆N₄OP₂]⁺: 1225.2655; found: 1225.2592. EA: calculated for C₆₄H₄₈CuF₆N₄OP₃: C: 63.05, H: 3.67, N: 4.08; found: C: 62.52, H: 3.69, N: 4.05.

4. Conclusions

Inspired by the great potential and the large variety of heteroleptic Cu(I) photosensitizers (CuPSs) this study presents the synthesis, structural and spectroscopic characterization of a systematic series of four novel Cu(I) complexes bearing different imidazo-phenanthroline ligands. Starting from 2-(4-bromophenyl)-1-phenyl-1*H*-imidazo-[4,5-*f*][1,10]phenanthroline (L2) the Suzuki cross-coupling reaction was used to extend the aromatic π-system and to introduce different substituents. The respective Cu(I) compounds were then prepared by a convenient one-pot two-step procedure in medium to high yields and fully structurally analyzed by several methods.

As a result of the extended π-system all Cu(I) complexes possess a significant cathodic shift >100 mV of their reduction potential compared to structurally related complexes without an imidazo moiety. Furthermore, the individual redox potentials are very similar and independent from the various substituents, which is a strong indication that the imidazo backbone is electronically decoupled from the phenanthroline sphere.

As another consequence the extended π-system causes redshifted metal-to-ligand charge transfer (MLCT) transition bands by more than 20 nm and increased extinction coefficients. These are both positive features, which contribute to a further improvement of heteroleptic CuPS as an alternative to noble metal-based systems in the future.

Finally, all complexes show a strong emission in the solid state and possess emission lifetimes of about 0.4 μs. This also qualifies these compounds for potential applications in OLEDs or LECs.

Supplementary Materials: The following are available online at <http://www.mdpi.com/2304-6740/6/4/134/s1>, Figures S1–S4: ¹H- and ¹³C-NMR spectra of C1–C4, Figures S5 and S6: High resolution ESI mass spectra of C1–C4, **Table S1:** Crystallographic data and refinement details of the complexes C1 and C2, **Figures S7 and S8:** The solid-state structures of C1 and C2, Figure S9: Emission lifetime measurements of C1–C4. The supplementary material also contains the CIF and the checkCIF output files of the complexes C1 and C2.

Author Contributions: Electrochemical and photophysical measurements, data analysis, visualization and manuscript writing, M.-A.S.; synthesis, data analysis and visualization, M.R.; X-ray measurements, W.F.; conceptualization, supervision, project administration, funding acquisition and manuscript writing, M.K. and S.T.

Funding: This research was founded by the Baden-Württemberg Foundation (BW-Stiftung, Stuttgart, Germany) and by the German Research Foundation (DFG, Bonn, Germany) via the Priority Program SPP 2102 “Light Controlled Reactivity of Metal Complexes” with the respective grant numbers TS 330/4-1 and KA 4671/2-1.

Acknowledgments: We gratefully acknowledge the synthetic work and support of Tatjana Basile.

Conflicts of Interest: The authors declare no conflict of interest.

References

1. Smalley, R.E. Future Global Energy Prosperity: The Terawatt Challenge. *MRS Bull.* **2005**, *30*, 412–417. [[CrossRef](#)]
2. Lewis, N.S.; Nocera, D.G. Powering the planet: Chemical challenges in solar energy utilization. *Proc. Natl. Acad. Sci. USA* **2006**, *103*, 15729–15735. [[CrossRef](#)]
3. Armaroli, N.; Balzani, V. The Future of Energy Supply: Challenges and Opportunities. *Angew. Chem. Int. Ed.* **2007**, *46*, 52–66. [[CrossRef](#)] [[PubMed](#)]
4. Schiermeier, Q.; Tollefson, J.; Scully, T.; Witze, A.; Morton, O. Electricity without Carbon. *Nature* **2008**, *454*, 816–823. [[CrossRef](#)] [[PubMed](#)]
5. Styring, S. Artificial photosynthesis for solar fuels. *Faraday Discuss.* **2012**, *155*, 357–376. [[CrossRef](#)] [[PubMed](#)]
6. Hammarström, L. Catalyst: Chemistry's Role in Providing Clean and Affordable Energy for All. *Chem* **2016**, *1*, 515–518. [[CrossRef](#)]
7. Service, R.F. Is It Time to Shoot for the Sun? *Science* **2005**, *309*, 548–551. [[CrossRef](#)] [[PubMed](#)]
8. Armaroli, N.; Balzani, V. Solar Electricity and Solar Fuels: Status and Perspectives in the Context of the Energy Transition. *Chem. Eur. J.* **2016**, *22*, 32–57. [[CrossRef](#)]
9. Armaroli, N. Photoactive mono- and polynuclear Cu(I)-phenanthrolines. A viable alternative to Ru(II)-polypyridines? *Chem. Soc. Rev.* **2001**, *30*, 113–124. [[CrossRef](#)]
10. Eckenhoff, W.T.; Eisenberg, R. Molecular systems for light driven hydrogen production. *Dalton Trans.* **2012**, *41*, 13004–13021. [[CrossRef](#)]
11. Frischmann, P.D.; Mahata, K.; Würthner, F. Powering the future of molecular artificial photosynthesis with light-harvesting metallosupramolecular dye assemblies. *Chem. Soc. Rev.* **2013**, *42*, 1847–1870. [[CrossRef](#)]
12. Yuan, Y.-J.; Yu, Z.-T.; Chen, D.-Q.; Zou, Z.-G. Metal-complex chromophores for solar hydrogen generation. *Chem. Soc. Rev.* **2017**, *46*, 603–631. [[CrossRef](#)]
13. Costa, R.D.; Ortí, E.; Bolink, H.J.; Monti, F.; Accorsi, G.; Armaroli, N. Luminescent Ionic Transition-Metal Complexes for Light-Emitting Electrochemical Cells. *Angew. Chem. Int. Ed.* **2012**, *51*, 8178–8211. [[CrossRef](#)]
14. Zhang, Y.; Schulz, M.; Wächter, M.; Karnahl, M.; Dietzek, B. Heteroleptic diamine-diphosphine Cu(I) complexes as an alternative towards noble-metal based photosensitizers: Design strategies, photophysical properties and perspective applications. *Coord. Chem. Rev.* **2018**, *356*, 127–146. [[CrossRef](#)]
15. Lazorski, M.S.; Castellano, F.N. Advances in the light conversion properties of Cu(I)-based photosensitizers. *Polyhedron* **2014**, *82*, 57–70. [[CrossRef](#)]
16. Housecroft, C.E.; Constable, E.C. The emergence of copper(I)-based dye sensitized solar cells. *Chem. Soc. Rev.* **2015**, *44*, 8386–8398. [[CrossRef](#)]
17. Dumur, F. Recent advances in organic light-emitting devices comprising copper complexes: A realistic approach for low-cost and highly emissive devices? *Org. Electron.* **2015**, *21*, 27–39. [[CrossRef](#)]
18. Weber, M.D.; Fresta, E.; Elie, M.; Miehlich, M.E.; Renaud, J.-L.; Meyer, K.; Gaillard, S.; Costa, R.D. Rationalizing Fabrication and Design Toward Highly Efficient and Stable Blue Light-Emitting Electrochemical Cells Based on NHC Copper(I) Complexes. *Adv. Funct. Mater.* **2018**, *28*, 1707423. [[CrossRef](#)]
19. Armaroli, N.; Accorsi, G.; Cardinali, F.; Cardinali, F. Photochemistry and Photophysics of Coordination Compounds: Copper. *Top. Curr. Chem.* **2007**, *69*–115. [[CrossRef](#)]
20. Tschierlei, S.; Karnahl, M.; Rockstroh, N.; Junge, H.; Beller, M.; Lochbrunner, S. Substitution-Controlled Excited State Processes in Heteroleptic Copper(I) Photosensitizers Used in Hydrogen Evolving Systems. *ChemPhysChem* **2014**, *15*, 3709–3713. [[CrossRef](#)]
21. Iwamura, M.; Takeuchi, S.; Tahara, T. Ultrafast Excited-State Dynamics of Copper(I) Complexes. *Acc. Chem. Res.* **2015**, *48*, 782–791. [[CrossRef](#)]
22. Mara, M.W.; Fransted, K.A.; Chen, L.X. Interplays of excited state structures and dynamics in copper(I) diimine complexes: Implications and perspectives. *Coord. Chem. Rev.* **2015**, *282–283*, 2–18. [[CrossRef](#)]
23. Paria, S.; Reiser, O. Copper in Photocatalysis. *ChemCatChem* **2014**, *6*, 2477–2483. [[CrossRef](#)]
24. Hernandez-Perez, A.C.; Collins, S.K. Heteroleptic Cu-Based Sensitizers in Photoredox Catalysis. *Acc. Chem. Res.* **2016**, *49*, 1557–1565. [[CrossRef](#)]
25. Luo, S.-P.; Mejía, E.; Friedrich, A.; Pazidis, A.; Junge, H.; Surkus, A.-E.; Jackstell, R.; Denurra, S.; Gladiali, S.; Lochbrunner, S.; Beller, M. Photocatalytic Water Reduction with Copper-Based Photosensitizers: A Noble-Metal-Free System. *Angew. Chem.* **2013**, *125*, 437–441. [[CrossRef](#)]

26. Mejía, E.; Luo, S.-P.; Karnahl, M.; Friedrich, A.; Tschierlei, S.; Surkus, A.-E.; Junge, H.; Gladiali, S.; Lochbrunner, S.; Beller, M. A Noble-Metal-Free System for Photocatalytic Hydrogen Production from Water. *Chem. Eur. J.* **2013**, *19*, 15972–15978. [[CrossRef](#)]
27. Balzani, V.; Juris, A.; Barigelletti, F.; Campagna, S.; Belser, P.; Von Zelewsky, A. Ru(II)-Polypyridine-complexes: Photophysics, Photochemistry, Electrochemistry and Chemiluminescence. *Coord. Chem. Rev.* **1988**, *84*, 85–277. [[CrossRef](#)]
28. Schäfer, B.; Görls, H.; Meyer, S.; Henry, W.; Vos, J.G.; Rau, S. Synthesis and Properties of Tetrasubstituted 1,10-Phenanthrolines and Their Ruthenium Complexes. *Eur. J. Inorg. Chem.* **2007**, 4056–4063. [[CrossRef](#)]
29. Troian-Gautier, L.; Moucheron, C. Ruthenium^{II} Complexes bearing Fused Polycyclic Ligands: From Fundamental Aspects to Potential Applications. *Molecules* **2014**, *19*, 5028–5087. [[CrossRef](#)]
30. Navarro, M.; Cisneros-Fajardo, E.J.; Sierralta, A.; Fernández-Mestre, M.; Silva, P.; Arrieché, D.; Marchán, E. Design of copper DNA intercalators with leishmanicidal activity. *J. Biol. Inorg. Chem.* **2003**, *8*, 401–408. [[CrossRef](#)]
31. Sandroni, M.; Maufroy, A.; Rebarz, M.; Pellegrin, Y.; Blart, E.; Ruckebusch, C.; Poizat, O.; Sliwa, M.; Odobel, F. Design of Efficient Photoinduced Charge Separation in Donor-Copper(I)-Acceptor Triad. *J. Phys. Chem. C* **2014**, *118*, 28388–28400. [[CrossRef](#)]
32. Heberle, M.; Tschierlei, S.; Rockstroh, N.; Ringenberg, M.; Frey, W.; Junge, H.; Beller, M.; Lochbrunner, S.; Karnahl, M. Heteroleptic Copper Photosensitizers: Why an Extended π -System Does Not Automatically Lead to Enhanced Hydrogen Production. *Chem. Eur. J.* **2017**, *23*, 312–319. [[CrossRef](#)]
33. Zhang, Y.; Traber, P.; Zedler, L.; Kupfer, S.; Gräfe, S.; Schulz, M.; Frey, W.; Karnahl, M.; Dietzek, B. Cu(I) vs. Ru(II) photosensitizers: Elucidation of electron transfer processes within a series of structurally related complexes containing an extended π -system. *Phys. Chem. Chem. Phys.* **2018**, *20*, 24843–24857. [[CrossRef](#)]
34. Soulis, K.; Gourlaouen, C.; Daniel, C.; Quatela, A.; Odobel, F.; Blart, E.; Pellegrin, Y. New luminescent copper(I) complexes with extended π -conjugation. *Polyhedron* **2018**, *140*, 42–50. [[CrossRef](#)]
35. Jin, C.; Liu, J.; Chen, Y.; Zeng, L.; Guan, R.; Ouyang, C.; Ji, L.; Chao, H. Cyclometalated Iridium(III) Complexes as Two-Photon Phosphorescent Probes for Specific Mitochondrial Dynamics Tracking in Living Cells. *Chem. Eur. J.* **2015**, *21*, 12000–12010. [[CrossRef](#)]
36. Jadhav, T.; Choi, J.M.; Lee, J.Y.; Dhokale, B.; Misra, R. Non-doped blue organic light emitting devices based on tetraphenylethylene- π -imidazole derivatives. *Org. Electron.* **2016**, *37*, 448–452. [[CrossRef](#)]
37. Kuang, S.-M.; Cuttell, D.G.; McMillin, D.R.; Fanwick, P.E.; Walton, R.A. Synthesis and Structural Characterization of Cu(I) and Ni(II) Complexes that Contain the Bis[2-(diphenylphosphino)phenyl]ether Ligand. Novel Emission Properties for the Cu(I) Species. *Inorg. Chem.* **2002**, *41*, 3313–3322. [[CrossRef](#)]
38. Fischer, S.; Hollmann, D.; Tschierlei, S.; Karnahl, M.; Rockstroh, N.; Barsch, E.; Schwarzbach, P.; Luo, S.-P.; Junge, H.; Beller, M.; et al. Death and Rebirth: Photocatalytic Hydrogen Production by a Self-Organizing Copper-Iron System. *ACS Catal.* **2014**, *4*, 1845–1849. [[CrossRef](#)]
39. Zhang, Y.; Heberle, M.; Wächtler, M.; Karnahl, M.; Dietzek, B. Determination of side products in the photocatalytic generation of hydrogen with copper photosensitizers by resonance Raman spectroelectrochemistry. *RSC Adv.* **2016**, *6*, 105801–105805. [[CrossRef](#)]
40. Wu, J.-Z.; Ye, B.-H.; Wang, L.; Ji, L.-N.; Zhou, J.-Y.; Li, R.-H.; Zhou, Z.-Y. Bis(2,2'-bipyridine)ruthenium(II) complexes with imidazo[4,5-*f*][1,10]-phenanthroline or 2-phenylimidazo[4,5-*f*][1,10]phenanthroline. *J. Chem. Soc. Dalton Trans.* **1997**, 1395–1402. [[CrossRef](#)]
41. Peuntinger, K.; Pilz, T.D.; Staehle, R.; Schaub, M.; Kaufhold, S.; Petermann, L.; Wunderlin, M.; Görls, H.; Heinemann, F.W.; Li, J.; et al. Carbene based photochemical molecular assemblies for solar driven hydrogen generation. *Dalton Trans.* **2014**, *43*, 13683–13695. [[CrossRef](#)]
42. Petermann, L.; Staehle, R.; Pfeifer, M.; Reichardt, C.; Sorsche, D.; Wächtler, M.; Popp, J.; Dietzek, B.; Rau, S. Oxygen-Dependent Photocatalytic Water Reduction with a Ruthenium(imidazolium) Chromophore and a Cobaloxime Catalyst. *Chem. Eur. J.* **2016**, *22*, 8240–8253. [[CrossRef](#)]
43. Hedley, G.J.; Ruseckas, A.; Samuel, I.D.W. Vibrational Energy Flow Controls Internal Conversion in a Transition Metal Complex. *J. Phys. Chem. A* **2010**, *114*, 8961–8968. [[CrossRef](#)]
44. Lennox, A.J.J.; Fischer, S.; Jurrat, M.; Luo, S.-P.; Rockstroh, N.; Junge, H.; Ludwig, R.; Beller, M. Copper-Based Photosensitizers in Water Reduction: A More Efficient In Situ Formed System and Improved Mechanistic Understanding. *Chem. Eur. J.* **2016**, *22*, 1233–1238. [[CrossRef](#)]

45. Shi, L.; Li, B. A Series of CuI Complexes Containing 1,10-Phenanthroline Derivative Ligands: Synthesis, Characterization, Photophysical, and Oxygen-Sensing Properties. *Eur. J. Inorg. Chem.* **2009**, *2009*, 2294–2302. [[CrossRef](#)]
46. Gottlieb, H.E.; Kotlyar, V.; Nudelman, A. NMR Chemical Shifts of Common Laboratory Solvents as Trace Impurities. *J. Org. Chem.* **1997**, *62*, 7512–7515. [[CrossRef](#)]
47. Bruker, S. *APEX2 and SAINT*; Bruker AXs Inc.: Madison, WI, USA, 2008.
48. Sheldrick, G.M. Crystal structure refinement with SHELXL. *Acta Crystallogr. C* **2015**, *71*, 3–8. [[CrossRef](#)]
49. Wilfred, L.A.; Christina, L.L.C. *Purification of Laboratory Chemicals*, 6th ed.; Butterworth–Heinemann: Oxford, UK, 2009; ISBN 978-1-85617-567-8.



© 2018 by the authors. Licensee MDPI, Basel, Switzerland. This article is an open access article distributed under the terms and conditions of the Creative Commons Attribution (CC BY) license (<http://creativecommons.org/licenses/by/4.0/>).